

A highly adaptive magnetorheological fluid robotic leg for efficient terrestrial locomotion

This content has been downloaded from IOPscience. Please scroll down to see the full text.

2016 Smart Mater. Struct. 25 095019

(<http://iopscience.iop.org/0964-1726/25/9/095019>)

View [the table of contents for this issue](#), or go to the [journal homepage](#) for more

Download details:

IP Address: 202.38.71.28

This content was downloaded on 12/07/2017 at 07:46

Please note that [terms and conditions apply](#).

You may also be interested in:

[Development of a novel variable stiffness and damping magnetorheological fluid damper](#)

Shuaishuai Sun, Jian Yang, Weihua Li et al.

[A Torsional MRE Joint for a C-Shaped Robotic Leg](#)

M D Christie, S S Sun, D H Ning et al.

[Theoretical and experimental study on a compliant flipper-leg during terrestrial locomotion](#)

Tao Fang, Youcheng Zhou, Shikun Li et al.

[Design and performance evaluation of a novel magnetorheological valve with a tunable resistance gap](#)

Guoliang Hu, Ming Long, Lifan Yu et al.

[Development of a semi-active dynamic vibration absorber for longitudinal vibration of propulsion shaft system based on magnetorheological elastomer](#)

Gaoyu Liu, Kun Lu, Donglin Zou et al.

[Characterization of running with compliant curved legs](#)

Jae-Yun Jun and Jonathan E Clark

[Development of an MR seat suspension with self-powered generation capability](#)

S S Sun, D H Ning, J Yang et al.

[A miniature MRE isolator for lateral vibration suppression of bridge monitoring equipment: design and verification](#)

Lujie Zhao, Miao Yu, Jie Fu et al.

[A semi-active magnetorheological fluid mechanism with variable stiffness and damping](#)

Christoph Greiner-Petter, Aditya Suryadi Tan and Thomas Sattel

A highly adaptive magnetorheological fluid robotic leg for efficient terrestrial locomotion

Nan Jiang¹, Shuaishuai Sun², Yiming Ouyang¹, Min Xu¹, Weihua Li² and Shiwu Zhang¹

¹Department of Precision Machinery and Precision Instrumentation, University of Science and Technology of China, Hefei, 230026, People's Republic of China

²School of Mechanical, Materials and Mechatronic Engineering, University of Wollongong, Wollongong, NSW 2522, Australia

E-mail: swzhang@ustc.edu.cn

Received 18 May 2016, revised 27 June 2016

Accepted for publication 19 July 2016

Published 9 August 2016



CrossMark

Abstract

To survive in nature, animals adjust the characteristics of their legs or fins to adapt the motion to their environment. Inspired by the locomotion of animals, a study on the tunable stiffness and damping of a leg will help in the development of intelligent locomotion robots. In this paper we report on the development and experiment of a novel and simple robotic leg that can be adapted to the environment via a smart magnetorheological fluid (MRF). The robotic leg consists of a rotation MRF damper, a torsional spring, a 'foot' and a 'leg'. The curved part of the 'foot' makes contact with the grounds while the other end is linked to an outer cylinder of the MRF damper with an inelastic cable. The variable force arm rising from the MRF damper and the torsional spring can help the leg adapt to a changing environment. The characteristics of the MRF damper have been investigated and a model is built to describe its mechanical features when different currents are applied to the MRF damper. A test on a linear dynamic test instrument has been conducted to verify the accuracy of the model. The robotic leg is installed in a locomotion platform to investigate the speed of its locomotion and the cost of the transport; the result demonstrated the feasibility and adaptability of the leg when walking on hard terrain. Its simple structure, high adaptability, and easy control of the MRF leg helped in the design and development of a high performance field robot that can adapt to various environments.

Keywords: locomotion, adaptive leg, magnetorheological fluid, cost of transport

(Some figures may appear in colour only in the online journal)

1. Introduction

As animals run, their tendons, ligaments, muscles and bones are coordinated to allow them to move over a large range of terrains. When animals move, the gravitational energy and kinetic energy are exchanged in each step [1]; in effect they use their muscles to generate periodic motion and asymmetric interaction forces to obtain forward acceleration with the environment, and these are two key principles [2]. A fast and effective locomotion involves interaction between the mechanisms and the environment. Research has revealed that a compliant leg rather than a stiff leg can reflect the dynamics of walking and running [3], which means that animals can adjust the mechanical properties of their legs to adapt to the real world

when they encounter changing terrains and tasks [4]. However, it has been proved that tuning leg stiffness could result in a better performance than simply controlling the gait [5].

Inspired by the mechanisms of animals that enable highly effective locomotion, many passive compliant legs have been developed and equipped with the dynamics of running robots such as Raibert's hoppers [6], RHex [7], Scout [8, 9], Whigs [10, 11] and AQUA [12]. A simple compliant leg may satisfy the purpose of limited locomotion in a certain range of conditions such as load, speed, gait, surface stiffness, and so forth, from which many researchers have introduced adaptable impedance into these platforms. Many attempts have also been made to develop legs and joints with variable stiffness for highly adaptive robots [13–16], but these changes can only be made

mechanically or manually, and even those robots who achieved better locomotion than robots with stiff legs, had an extremely complex mechanical structure and a limited response frequency.

There are four ways to control the structural mechanisms; passive control, active control, hybrid control, and semi-active control, respectively. The main difference between passive control and active control is that an active control system requires an external power source that applies to the structure, while the other does not. A hybrid control system, as the name implies, is a combination of passive and active control systems, while a semi-active control device only needs external energy which is not like the mechanical energy in an active control system [17]. Magnetorheological fluid (MRF) is a kind of smart material which can respond immediately and dramatically to an applied magnetic field [18]. An MRF damper is semi-active control, so it has the advantages of active and passive control, while being more convenient than passive control, and requires less energy than active control.

The characteristics of MRF are rapid response, reversible transition, and a simple control strategy on the mechanical structure which allows it to be applied extensively, at least up to now [19]. Dyke *et al* [20], and Li *et al* [21] have carried out many interesting studies on an MRF damper and also developed several models to describe the mechanical properties [22, 23] of MRF. Furthermore, a variable stiffness damper that absorbs vibration using MRF [24] has been developed, where the stiffness is tunable by the current. These remarkable properties make adjusting the mechanical properties of robotic legs with MRF devices intuitive.

This paper describes the design and subsequent experiment of a highly adaptive robot leg combined with an MRF device where the leg uses the MRF damper to adjust its compressing distance and change its compressing force as it moves along the ground; it does this by changing the force arm, which is related to the compressing distance of the leg. Most importantly, the compressing force can be controlled through the MRF damper because the damping force can be changed by applying different currents. This adaptive leg overcomes the high energy consumption and complex structure of a traditional mechanical leg of variable stiffness, and can potentially be applied to terrestrial and amphibious robots to increase their locomotion over various terrains.

The remainder of this paper is as follows. Section 2 introduces the structure of this adaptive leg and the relationship curves between the compressing force and vertical displacement. Section 3 develops a theoretical model by which the vertical compressing force can be deduced and the related parameters determined. Section 4 introduces an experimental setup for the adaptive leg and states its locomotory performance under different currents and angular velocities. Section 5 summarizes the advantages of this adaptive leg and describes the future work.

2. Design of MRF leg

An MRF damper is generally used to absorb vibration because its damping force can be changed in different

magnetic fields, but it can also be used in other fields such as adjusting the mechanical properties of a robotic leg. Moreover, the forces activated during locomotion on various terrains can be controlled by adjusting the properties of the leg.

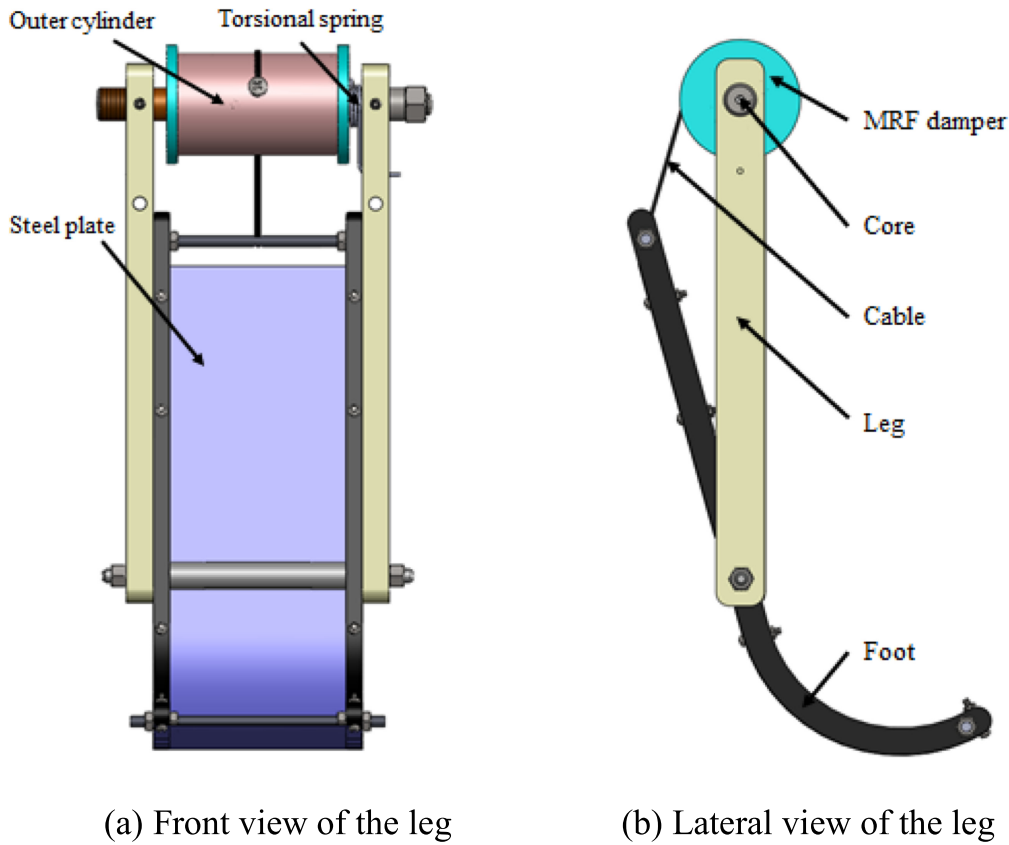
2.1. Structure of the highly adaptive leg

The conceptual design of this adaptive leg is presented in figure 1. It consists of a curved 'foot,' a straight 'leg,' a cable, an MRF damper, a core axle, a steel plate, and a torsional spring. The curved 'foot' provides forward and supportive force, just like the curved legs of the RHex and Amphihex robots. The straight 'leg' supports the MRF damper and provides a pivot for the 'foot.' The outer cylinder of the MRF damper is linked to the 'foot' through an inelastic cable. A 0.2 mm thick steel plate is connected to the 'foot' to allow it to adapt to a wider range of terrain. As it walks, the 'foot' rotates to form an angle between the core and outer cylinder of the damper, while the forces acting on the 'foot' vary according to the synthesized effect of the driving torque of the motor on the axle, the damper force of the MRF damper, and the dynamic force of the terrain acting on the 'foot'. In order to return to an original state when a stride is finished, a torsional spring is fitted between the side cover of the damper, while the 'leg' is attached to the core. A torsional spring with an initial rotational angle of $\pi/60$ exerts a small compressing force onto the leg when no current has been applied onto the damper, so a maximum angle between the core and the side cover is controlled by the torsional spring to enable the leg to have a suitable end position.

The cable is connected to the outer cylinder of the MRF damper and the 'foot' so that the 'foot' acts like a human foot as it makes contact with the ground. The 'leg' only supports the 'foot' and the damper, and is connected to the outer cylinder of the damper via a torsional spring.

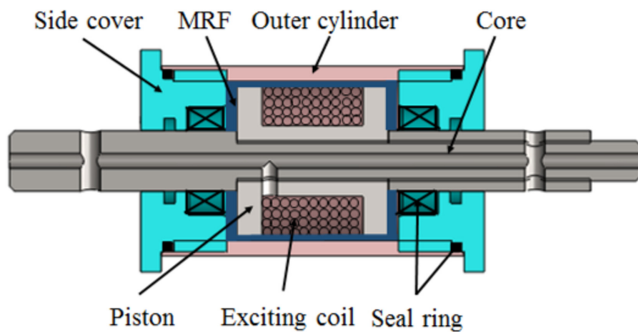
The MRF damper can provide a real time damping force by adjusting the applied current on its exciting coil. The structure of the MRF damper is shown in figure 2, where it consists of two side covers, an outer cylinder, an excitation coil, a piston, sealing rings, and a core. The piston is fixed to the 'leg' through the core, which can rotate with the 'leg' during a stride. The magnetic circuit consists of an external cylinder, the piston, and the exciting coil. The MRF between the external cylinder and the piston exhibits a Newtonian type of behavior when there is no magnetic field applied, but a magnetic field is applied by the exciting coil, several magnetic chains are formed in the direction of magnetic induction, and then a shear stress is formed when there is a shear move between the external cylinder and the piston. This behavior can be represented as a Bingham model [25]. During a stride the 'foot' makes contacts with the ground and rotates around the axle as the 'leg' rotates. The cable is tightened and rotates the external cylinder around the inner core of the damper, after which a torque is produced that prevents rotation. The most remarkable characteristic of this damper is that the torque can be changed in milliseconds by altering the current.

The core and the piston are united into one part, and the core is fixed to the 'leg'. The external cylinder has two side



(a) Front view of the leg

(b) Lateral view of the leg

Figure 1. Mechanical structure of the highly adaptive leg.**Figure 2.** Design of the rotational MRF damper.

covers and is connected to the 'foot' with a cable. The MRF is full of the inner space between the external cylinder, the side covers, and the piston.

The design of the highly adaptive leg allow the mechanical properties to be adjusted by controlling the current during locomotion. Compared to other tunable stiffness legs, this highly adaptive leg can not only control the compressing force in the same position as a tunable stiffness leg, it also consumes less energy than active control.

2.2. Analysis of the rotational MRF damper

The MRF damper is the most important component of this highly adaptive leg because its viscosity increases with the

density of magnetic flux, which means the density of this MRF damper must be analyzed. The magnetic circuit of the rotational MRF damper is shown in figure 3 and the related parameters are listed in table 1. In figure 3, d_1 is the diameter of the core, d_2 is the diameter of the center of the piston, d_3 is the diameter of the side of the piston, h_1 is the magnetic resistance gap of the MRF between the side of the piston and the external cylinder, h_2 is the thickness of the outer cylinder, l_1 is the length of the side of the piston, l_2 is the length of exciting coil, l_3 is the length of the piston.

The coil in the MRF damper has approximately 210 turns and the density of the MRF used in the damper is 2.5828 g cm^{-3} , the external cylinder and the piston are manufactured from 20 grade steel, and the relationship between the density of magnetic flux B to the density of magnetic field H of the MRF and the 20 grade steel are shown in figure 4, respectively. To prevent an unbalanced force from forming along the core, and to reduce the weight of the leg, the side covers are made from aluminium. The magnetic resistance of the center of piston can be calculated as shown below:

$$R_1 = \frac{l_1 + l_2}{\pi [(d_2/2)^2 - (d_1/2)^2] \mu_1 \mu_0}, \quad (1)$$

where μ_1 is the relative permeability of the piston, μ_0 is the permeability of the vacuum. The magnetic resistance of the

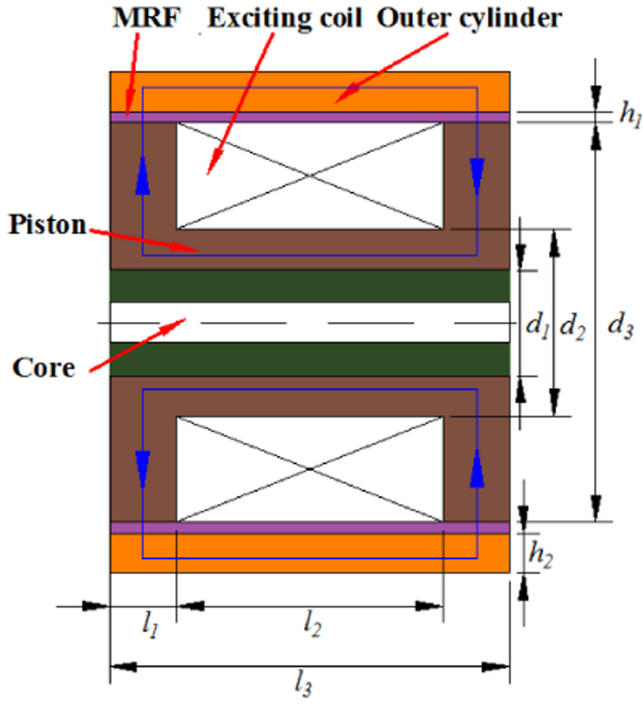


Figure 3. Sketch of the rotational MRF damper.

Table 1. Parameters for rotational MRF damper.

Parameters	Value	Parameters	Value
d_1	8 mm	h_2	3 mm
d_2	14 mm	l_1	5 mm
d_3	30 mm	l_2	20 mm
h_1	0.8 mm	l_3	30 mm

side of the piston can be calculated as shown below:

$$R_2 = \frac{(d_3 - d_1)/2}{\pi [(d_1 + d_3)/2] l_1 \mu_1 \mu_0}. \quad (2)$$

The magnetic resistance of the MRF gap can be calculated as shown below:

$$R_3 = \frac{h_1}{\pi (d_3 + h_1) l_1 \mu_2 \mu_0}, \quad (3)$$

where μ_2 is the relative permeability of MRF. The magnetic resistance of the external cylinder can be calculated as shown below:

$$R_4 = \frac{l_1 + l_2}{\pi [(d_3/2 + h_1 + h_2)^2 - (d_3/2 + h_1)^2] \mu_0 \mu_1}. \quad (4)$$

Thus the total magnetic resistance can be deduced as shown below:

$$R_m = R_1 + 2R_2 + 2R_3 + R_4. \quad (5)$$

Therefore, the magneto-motive force which is based on Ohm's Law can be given by

$$NI = B_0 S_0 R_m, \quad (6)$$

where B_0 is the density of magnetic flux of the resistance gap and S_0 is the flux area of the resistance gap.

In the MRF damper, the active area, which is the gap h_1 between the piston and the external cylinder, plays an important role in altering the damping force. Based on this above analysis, the density of magnetic flux in the active area under different currents can be deduced by FEM, as shown in figure 5. The density of flux in the active area will reach saturation in 2 A, and then three different currents 0, 0.5, and 2 A are used in the following experiments.

2.3. Test of the highly adaptive leg

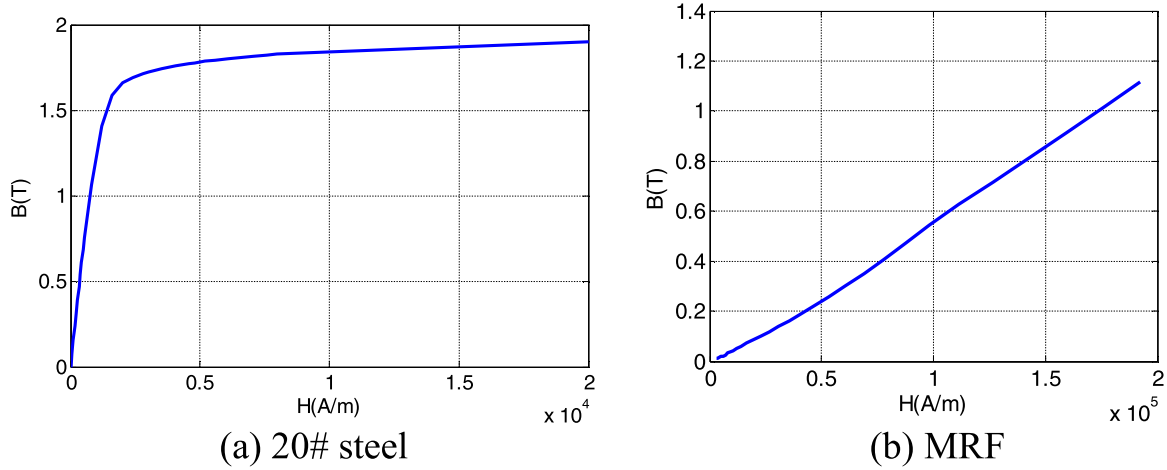
To measure the property of the leg, the relationship between the vertical force and vertical displacement must be obtained. A linear dynamic test instrument (INSTRON E3000) is used to measure the vertical displacement and relative force. The leg testing experimental apparatus is presented in figure 6. The leg and a clamp are assembled together, with one side of the clamp fixed on the top side of the instrument, which can generate a vertical motion, and the other side is fastened to the highly adaptive 'leg'. When the upper side of the apparatus provides a vertical motion that was programmed to a certain velocity and frequency, the 'foot' of the highly adaptive leg always moves along the bottom plate which is fixed on the pressure sensor, thus the vertical force can be measured at this relative position.

To obtain the results of these universal experiments, four methods were chosen to control the velocity; two constant velocities with 2 and 3 mm s⁻¹, and two constant frequencies with 0.125 and 0.25 Hz. The test results are presented in figure 7.

Based on these test results, the compressing force increases when the clamp moves downwards, and the force returns to zero when the 'foot' leaves the plate while the clamp moves upwards. It is easy to see here that the compressing forces is always consistent with the same current and velocity even though the ends are different, and the compressing forces increase with different slopes when the applied current is changed. Thus, the leg can perform similar to a tunable stiffness leg with a simple control method.

3. Dynamic model and parameter identification

Based on the design of the leg, stiffness in a lateral direction can be considered as a large constant with a rigid structure; this design can avoid an unsteady stride in a lateral direction so all we need to consider is the force in the sagittal plane. A dynamic model was build and the related parameters were fitted in the next part.

Figure 4. B - H curve.

3.1. Dynamic model of the highly adaptive leg

According to this design, the compressing force helps the 'leg' move forward during a stride, so we can then focus on the compressing force which can be calculated on the assumption that the 'leg' moves along the negative Y -axis, and the arch of the 'foot' always moves along the ground. Obviously, the cable and the external cylinder are consistently on a tangent because the cable is always longer or shorter along the surface of the external cylinder.

The geometric relationship of the leg must be deduced in the model, so a simplified structure of the leg in the sagittal plane is presented in figure 8, and the related parameters are listed in table 2.

The relationship between the length of cable L_2 and θ can be calculated as below.

$$L_2 = \sqrt{L_1^2 + L_3^2 - 2L_1L_3 \sin \theta - r^2}. \quad (7)$$

The change in length of L_2 named D_{L2} can be deduced as

$$D_{L2} = L_2 |(\theta = \theta_i) - L_2|(\theta = \theta_0), \quad (8)$$

where $\theta_0 = \arccos(r/L_3)$. Accordingly, we can obtain the relationship between θ and β as shown below:

$$r \sin \beta + L_2 \cos \beta = L_3 \cos \theta \quad (9)$$

then we can obtain the relationship between unknown variables θ and β through equations (7) and (9) as shown below:

$$r \sin \beta + \sqrt{L_1^2 + L_3^2 - 2L_1L_3 \sin \theta - r^2} \cos \beta = L_3 \cos \theta \quad (10)$$

and the relationship between L_v and θ can also be calculated as

$$L_v = L_0 - [L_4 \sin \theta + R(1 - \cos \theta)], \quad (11)$$

where L_0 is the initial height of the leg, which can be calculated as $L_0 = L_4 \sin \theta_0 + R(1 - \cos \theta_0)$. L_v is the vertical displacement when the leg is compressed along the y -axis.

To obtain the compressing force on the ground, a force analysis of the 'foot' is shown in figure 9, where a ratio between the vertical force F_y applied by the ground and the vertical force decomposed from F_2 always exists with rotation around the pivot O of the 'foot'. So the arms from the force point of F_y and F_2 to the pivot O can be deduced as

$$\begin{cases} L_{1f} = L_4 \cos \theta + R \sin \theta, \\ L_{1s} = L_4 \sin \theta + R(1 - \cos \theta), \\ L_{2f} = L_3 \cos \theta, \\ L_{2s} = L_3 \sin \theta, \end{cases} \quad (12)$$

where L_{1f} and L_{1s} represent the force arm of F_y and F_x to the pivot O , L_{2f} and L_{2s} represent the force arm of the vertical and horizontal component force of F_2 by the cable to the pivot O .

The 'foot' is made from low density carbon fiber with 54 g, so the moment of inertia to the pivot O can be ignored. Then F_y , based on the moment equilibrium, can be deduced as shown below:

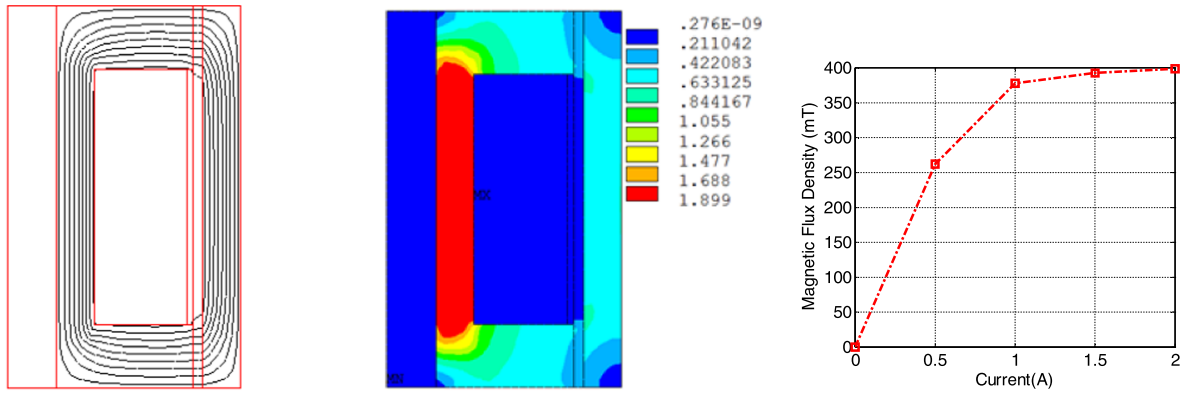
$$F_y = F_2 \cdot \frac{\sin \alpha \cdot L_{2f}}{L_{1f}} - T_f \cdot \frac{1}{L_{1f}} = a \cdot F_2 - b \cdot T_f, \quad (13)$$

where T_f is the initial moment of the leg, a is a coefficient that represents $\sin \beta \cdot L_{2f} / L_{1f}$ and b represents $1 / L_{1f}$. The values of a and b under vertical displacement are shown in figure 10 where $b \cdot T_f$ is represented as a constant if $b \cdot T_f$ is smaller than $a \cdot F_2$.

A mechanical model is used to describe the damping force [26], and then F_2 can be modeled based on the Bingham model, as shown in figure 11, which was caused by the MRF damper and the assembled torsional spring. Then the pull force F_2 applied by the cable can be written as

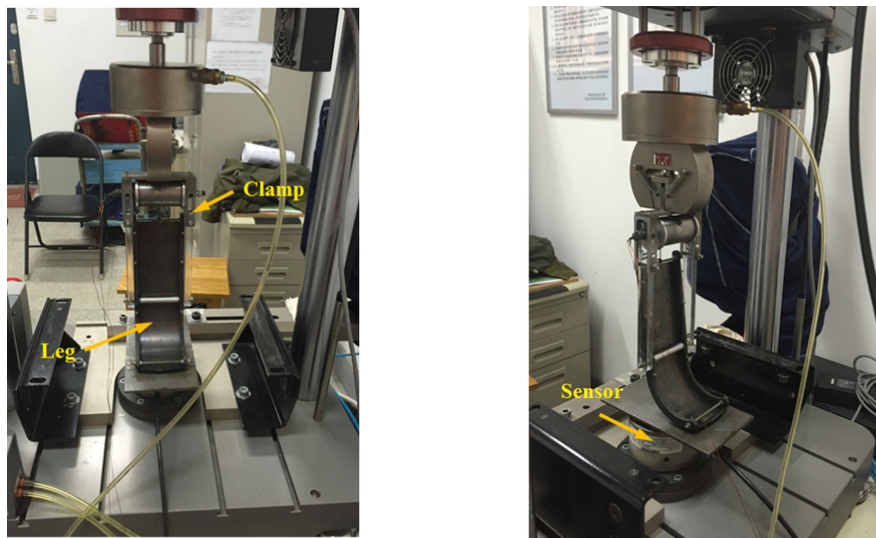
$$F_2 = k_s \cdot L_v + \text{sign}(\dot{L}_v) \cdot f_c + c \cdot \dot{L}_v + F_s, \quad (14)$$

where c is the damping coefficient and f_c is the coulomb friction force in the damper controlled by the current, \dot{L}_v is the first derivative of the L_v to the time, F_s is the preloading force of the torsional spring, which is 5 N, k_s is the stiffness of the equivalent compressed spring, which is converted from the torsional spring stiffness which is 11.065 N mm/($^\circ$), and k_s is calculated as $k_s = 3.306 \text{ N mm}^{-1}$.



(a) Magnetic flux line distribution (b) Magnetic flux density distribution (c) Flux density of the active area

Figure 5. FEM analysis of the MRF damper.



(a) Front view of the experimental setup (b) Side view of the experimental setup

Figure 6. Experimental setup to test the properties of the adaptive leg. The pressure sensor can measure the vertical force. The bottom plate is coated with vaseline to reduce the frictional force while the 'foot' moves on the plate.

Thus, the final vertical force applied by the ground can be calculated as shown below:

$$F_y = a \cdot (k_s \cdot L_v + \text{sign}(\dot{L}_v) \cdot f_c + c \cdot \dot{L}_v + F_s) - F_c, \quad (15)$$

where F_c is the mechanical friction force between the 'foot' and the 'leg' which is equal to $b \cdot T_f$.

3.2. Parameter identification

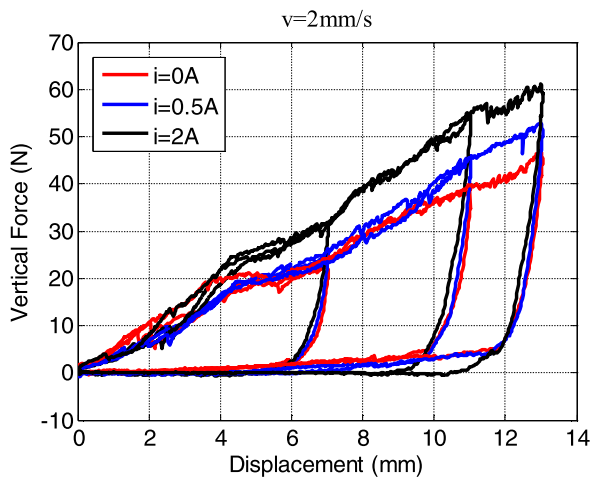
In order to assess the validity of the model, we fitted it with data measured from the test, as shown in figure 12. The unknown parameters of c , f_c and F_c in the model were determined by the least square method in MATLAB (R2010a), as shown in equation (16), where the minimum average square of the difference between the test data and model data was reached, and the identification of four different velocity control modes under the same current were

also the same. The parameters identified are listed in table 3.

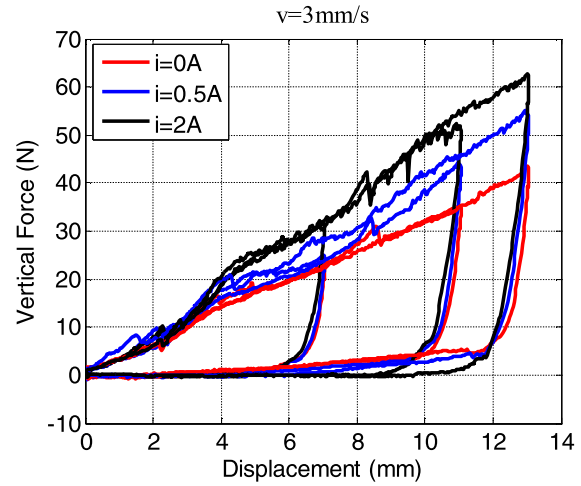
$$\min : J = \sum_{i=1}^n \frac{(F_m - F_y)^2}{n}, \quad (16)$$

where F_m is the predicted model data, F_y is the test data in the experiment, and n is the number of data points.

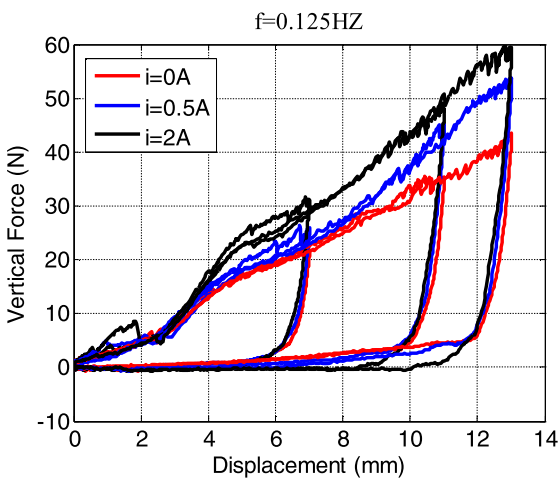
The unsteadiness of the test data mainly lies in the friction between the 'foot' and the bottom plate of the test apparatus, so there was always a creeping phenomenon in the experiments. However, all the parameters identified in the dynamic model increased as the current increased, the damping coefficient c increased slightly, and the coulomb friction increased rapidly with the current, so it can be concluded that the change velocity had very little effect on the vertical force, but as the current increased, the coulomb friction increased enough to keep the vertical force increasing monotonically.



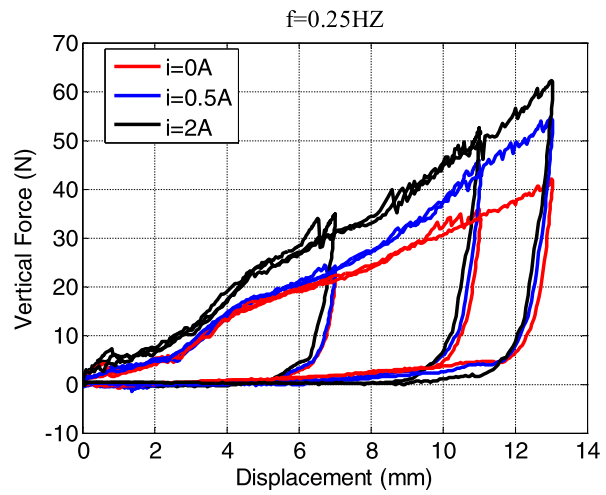
(a) Compression force at a speed of 2 mm/s



(b) Compression force at a speed of 3 mm/s



(c) Compressing force at a frequency of 0.125 Hz



(d) Compressing force at a frequency of 0.25 Hz

Figure 7. The relationship between the compressing force and vertical displacement with different methods of controlling the velocity under different currents. The maximum vertical displacement is 7 mm, 11 mm, and 13 mm, respectively.

4. Dynamic locomotion testing

In order to investigate the locomotion of the highly adaptive leg, an experimental platform similar to a wheel-terrain test bed [27] was set up. The locomotion of the leg can be evaluated with various controlling strategies and kinematic parameters.

4.1. Experimental locomotion platform

The experimental platform is shown in figure 13. The driving module (figure 13(b)) is assembled as one unit that can move vertically through two of four rolling translational guides. The other two translational guides were used to the platform move forwards as the highly adaptive leg rotated in the tank. The tank is 1850 mm × 800 mm × 500 mm (length × width × depth). To meet the torque requirement while the leg rotates at the designed angular velocity, a gear

box with a 2:1 ratio is mounted between the shaft of the leg and the motor, a torque sensor (range: 20 N m with accuracy: 0.5% F.S) that is connected to the output shaft of the gear box and the leg is used to measure the output torque of the driving module. An angular velocity of 1 and 2 rad s⁻¹ was selected to investigate the effects of rotating speed.

To identify the advantages of the highly adaptive leg, an evaluation criterion called the cost of transport (COT) [28, 29] was defined to represent consumption of the leg divided by weight times velocity

$$\text{COT} = \frac{\bar{P}}{mg\bar{v}}, \quad (17)$$

where m denotes the mass of the sum of leg and driving module, \bar{v} denotes the average speed of the driving module. \bar{P} is the average power cost in a stride, which can be calculated by multiplying the angular velocity of the leg and the torque T_c .

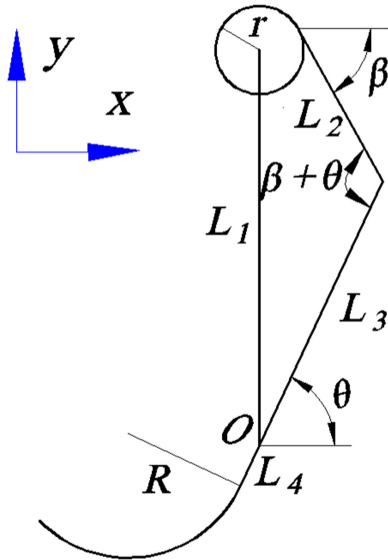


Figure 8. Geometric relationship of the leg in the sagittal plane. r and R represent the radius of the external cylinder and the arch of the ‘foot’ respectively. L_1 and L_2 represent the length of the ‘leg’ and the cable, respectively. L_3 and L_4 represent the length from both ends of the straight line of the ‘foot’ to the pivot of the ‘foot’, respectively. β represents the angle between the cable and the positive X -axis, and θ represents the angle between the straight part of the ‘foot’ and the positive X -axis.

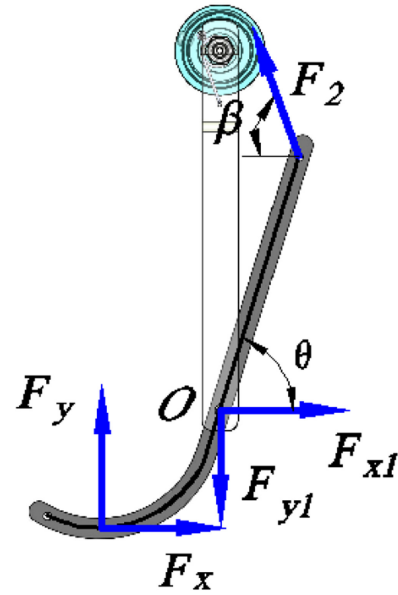


Figure 9. Force analysis of the ‘foot’. F_y and F_x are the vertical force and horizontal force respectively from the ground. F_{y1} and F_{x1} are the vertical force and horizontal force that are applied onto the pivot O by the ‘leg’. F_2 is the pull force from the cable.

Table 2. Parameters for the highly adaptive Leg.

Parameters	Value	Parameters	Value
L_1	175 mm	R	55 mm
L_3	129 mm	L_4	20 mm
Weight	732 g	r	22.8 mm
Arc angle	110°	Resistance of the MRF damper per R_c	2.6 Ω

4.2. Controlling strategy

The change of the output torque with zero applied current when the leg rotates in 1 and 2 rad s⁻¹ is presented in figure 14. The leg does not contact the ground during the first half stride, so it can return to its original state during that period. In the next half stride, the leg contacts the ground from π to $3\pi/2$ where the leg is compressed, so a current can now be applied to change the mechanical properties of the leg. Moreover, the torque has measured increases to a maximum value from π to $7\pi/6$ approximately, and decreases from $7\pi/6$ to $3\pi/2$, so this interval can be divided into three parts, as shown in figure 14. To compare the MRF damping leg with the same angular velocity, seven controlling strategies are defined, as shown in figure 15. No current applied on the MRF damper was control strategy 1. Applying constant currents of 0.5 A and 2 A were called controlling strategy 2 and 3, respectively. Moreover, to compare the variable currents and constant current in a stride, experiments where the

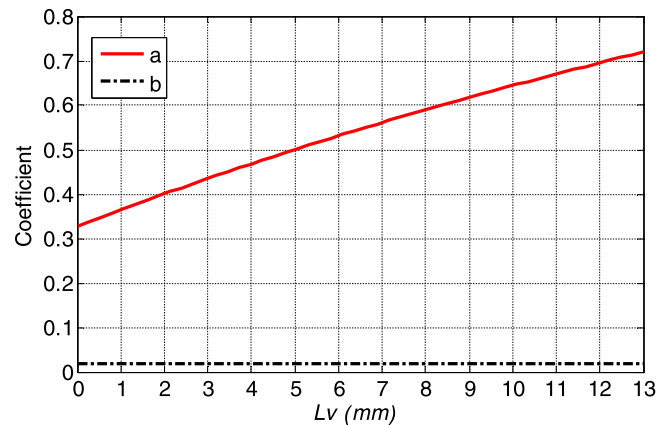


Figure 10. Ratio of vertical force on the ground and the damping force.

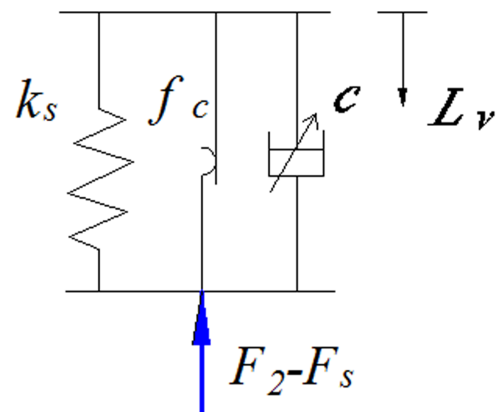
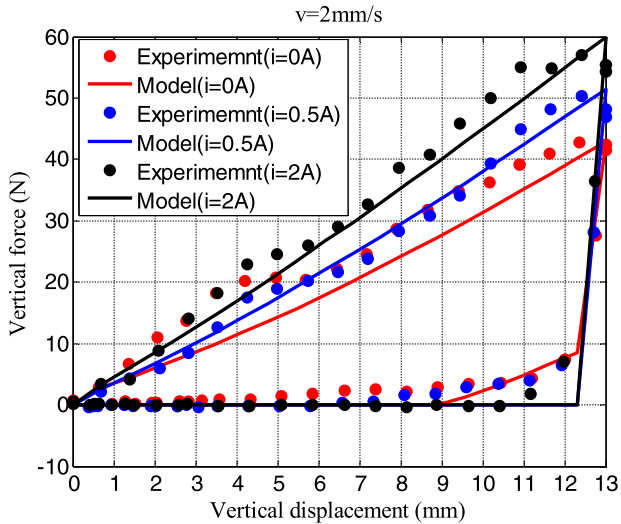
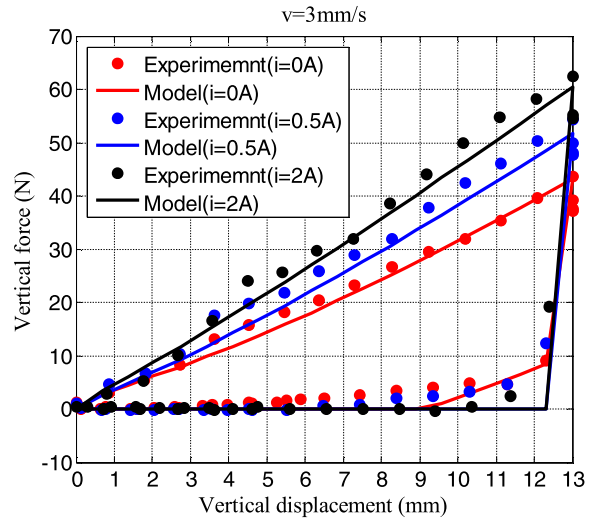


Figure 11. Mechanical model of the highly adaptive leg.



(a) Identification results at a speed of 2 mm/s



(b) Identification results at a speed of 3 mm/s

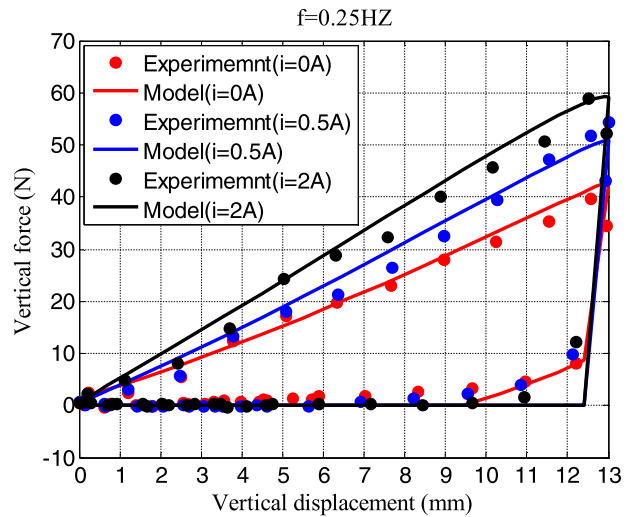
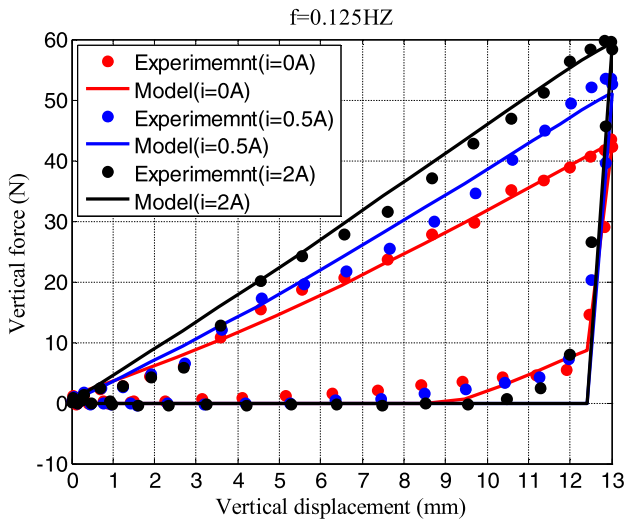


Figure 12. Identification results under different velocity control methods and currents.

Table 3. Parameter identification of the highly adaptive leg under different current (I).

	$i = 0 \text{ A}$	$i = 0.5 \text{ A}$	$i = 2 \text{ A}$
$c \text{ (N s mm}^{-1}\text{)}$	0.22	0.36	0.66
$f_c \text{ (N)}$	22.10	45.88	66.73
$F_c \text{ (N)}$	7.72	16.6	23.45

current varied from 0 to 2 A were also carried out (controlling strategies 4–7).

The current I at different controlling strategy can be represented as shown below:

$$I = \begin{bmatrix} 0 & 0 & 0 & 0 & 0 & 0 & 0 \\ 0 & 0.5 & 2 & 2 & 0.5 & 2 & 0 \\ 0 & 0.5 & 2 & 1.5 & 1 & 2 & 0 \\ 0 & 0.5 & 2 & 1 & 1.5 & 0 & 2 \\ 0 & 0.5 & 2 & 0.5 & 2 & 0 & 2 \end{bmatrix} \quad (18)$$

then the average power that the leg cost in a stride can be calculated as

$$\bar{P}_j = \frac{\int_0^T T_c \omega dt + \sum_{i=2}^{i=4} I_{(i,j)}^2 R_c \cdot \pi / (6\omega) + I_{(5,j)}^2 R_c \cdot \pi / (2\omega)}{T} \quad (19)$$

where j represents the control strategy.

4.3. Experimental results

The speed and COT of the experiments are recorded and calculated to evaluate the locomotion of the adaptive leg. The average forward speed is shown in figure 16. We can see that the speed increases when the leg runs with a higher angular velocity, and the forward velocity is almost the same when the leg runs at a lower angular velocity. The results indicate that the current applied in a stride only affects locomotion at a high angular velocity, and the controlling strategy 4 can reach the highest speed. The

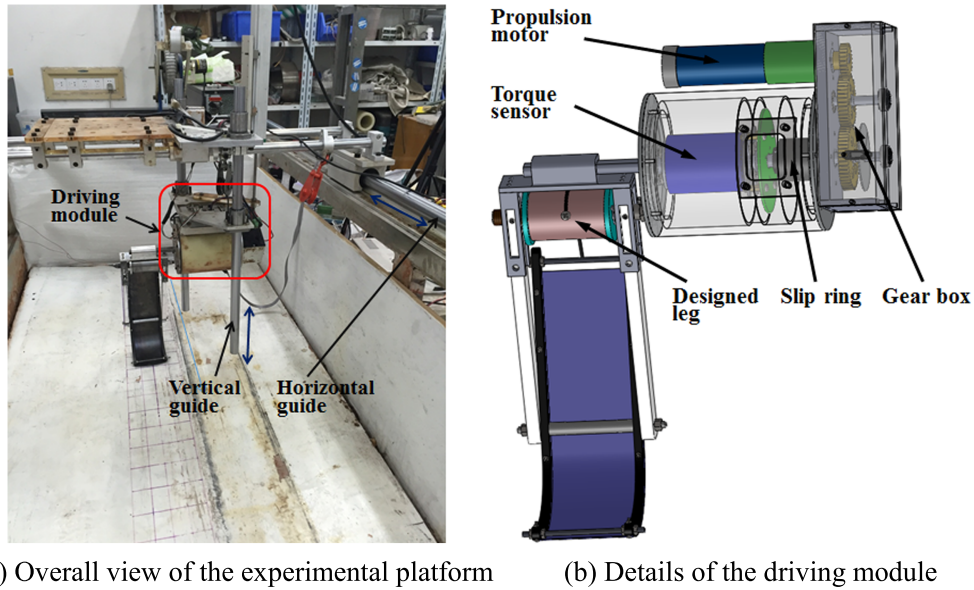


Figure 13. Experimental platform of the highly adaptive leg.

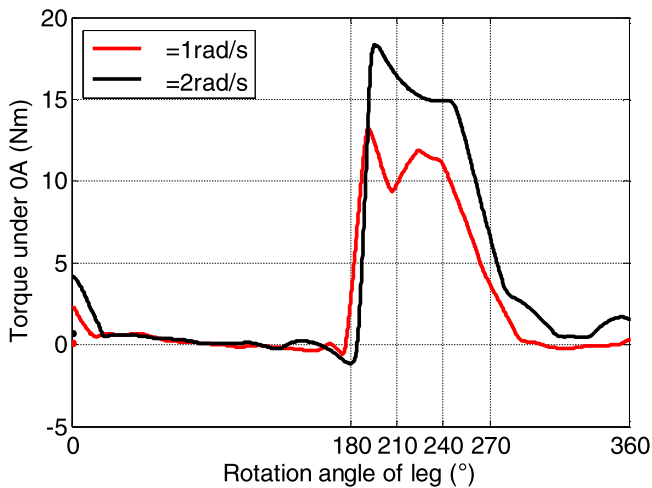


Figure 14. Torque with no current applied under different angular velocities.

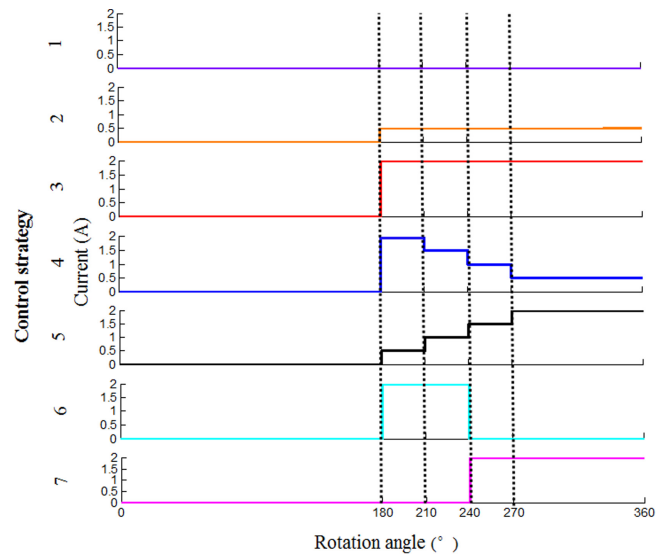


Figure 15. Controlling strategy in a stride.

COT at different controlling strategies under different angular velocities is shown in figure 17 where the controlling strategy 1 has the lowest COT because no other outside energy has been applied onto the leg, and controlling strategy 3 consumed the largest COT in a stride. However, controlling strategy 1 had the lowest speed. Compared to a constant current in the compression phase, controlling strategies 4, 5, 6, and 7 performed better, while controlling strategy 4 achieved the highest speed and relatively low COT in a stride. The experiment results indicated that the varied vertical force in a stride performed better when a constant current is applied to the leg in a stride. This indicates that the MRF damping leg can perform better when the robot encounters a changing environments or tasks, which will explore the applications of the field robots in future.

5. Conclusions

Compliant legs with a constant stiffness have been studied for a long time, but to obtain better locomotion means they must be similar to animals running in the wild. While many excellent works on tunable stiffness legs has been done, most only realize changes in vertical force mechanically, so a vertical force cannot be turned in real time and its controlling strategy is very complex.

In this paper we have presented the design and locomotion experiments of a highly adaptive leg based on MRF. The simple controlling method and the rapid response of these legs will enable robots to adapt to their environments and tasks. The experiment results showed that the leg we designed can perform better at a high angular speed, and unlike other tunable legs, its vertical force can change in real time to adapt

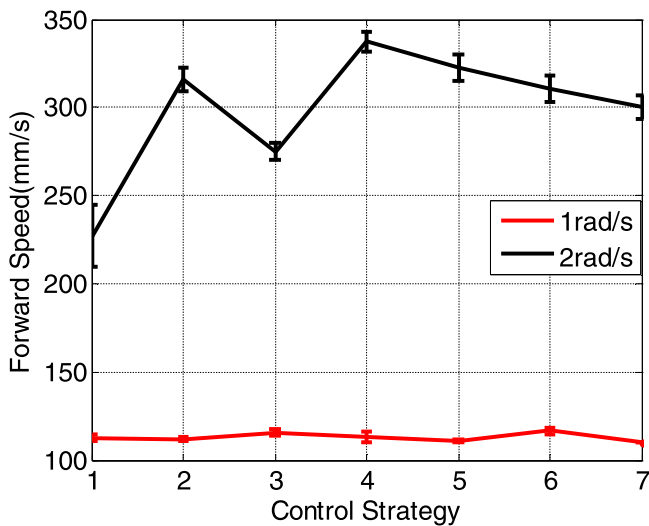


Figure 16. Forward speed in different control strategies under different angular velocities.

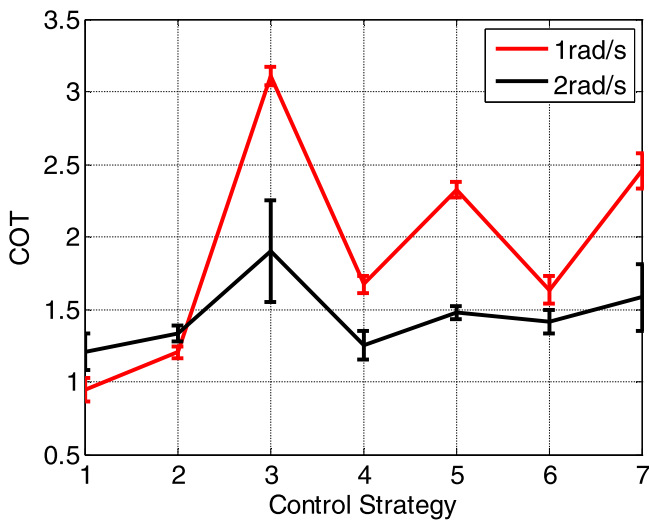


Figure 17. COT in different control strategies under different angular velocities.

to its surroundings whilst under semi-active control. Moreover, the assumption that a highly adaptive leg is lower at a higher angular velocity compared to a mechanically tunable stiffness leg is incorrect.

In the future, the vertical force can be changed over a larger range by optimizing the structure of the MRF damper and the leg, and the locomotion of the leg in more complex environments such as muddy terrain and sandy terrain should also be explored.

Acknowledgments

This research is supported by National Natural Science Foundation of China (No. 51375468). The authors would like to thank Mr Zhuo Chen, Mr Ya Wu, and Ms Zijun Jing for their help in setting up the experimental platform and in conducting the experiments.

References

- [1] Dickinson M H, Farley C T, Full R J, Koehl M A R, Kram R and Lehman S 2000 How animals move: an integrative view *Science* **288** 100–6
- [2] Ijspeert A J 2014 Biorobotics: using robots to emulate and investigate agile locomotion *Science* **346** 196–203
- [3] Geyer H, Seyfarth A and Blickhan R 2006 Compliant leg behaviour explains basic dynamics of walking and running *Proc. R. Soc. B* **273** 2861–7
- [4] Ferris D P, Louie M and Farley C T 1998 Running in the real world: adjusting leg stiffness for different surfaces *Proc. R. Soc. B* **265** 989–94
- [5] Jun J Y and Clark J E 2009 Dynamic stability of variable stiffness running *ICRA: IEEE Conf. on Robotics and Automation* pp 1756–61
- [6] Raibert M H 1986 *Legged Robots that Balance* (Cambridge, MA: MIT Press)
- [7] Saranli U, Buehler M and Koditschek D E 2001 RHex: a simple and highly mobile hexapod robot *Int. J. Robot. Res.* **20** 616–31
- [8] Buehler M, Battaglia R, Cocosco A, Hawker G, Sarkis J and Yamazaki K 1998 SCOUT: a simple quadruped that walks, climbs, and runs *ICRA: IEEE Conf. on Robotics and Automation* pp 1707–12
- [9] Poulakakis I, Smith J A and Buehler M 2005 Modeling and experiments of untethered quadrupedal running with a bounding gait: the Scout II robot *Int. J. Rob. Res.* **24** 239–56
- [10] Harkins R, Ward J, Vaidyanathan R, Boxerbaum A S and Quinn R D 2005 Design of an autonomous amphibious robot for surf zone operations: part II—hardware, control implementation and simulation *AIM: IEEE/ASME Conf. on Advanced Intelligent Mechatronics* pp 1465–70
- [11] Boxerbaum A S, Klein M A, Bachmann R, Quinn R D, Harkins R and Vaidyanathan R 2009 Design of a semi-autonomous hybrid mobility surf-zone robot *AIM: IEEE/ASME Conf. on Advanced Intelligent Mechatronics* pp 974–9
- [12] Dudek G et al 2007 Aqua: an amphibious autonomous robot *Computer* **40** 46–53
- [13] Wolf S and Hirzinger G 2008 A new variable stiffness design: matching requirements of the next robot generation *ICRA: IEEE Conf. on Robotics and Automation* pp 1741–6
- [14] Toniatti G, Schiavi R and Biechi A 2005 Design and control of a variable stiffness actuator for safe and fast physical human/robot interaction *ICRA: IEEE Conf. on Robotics and Automation* pp 526–31
- [15] Galloway K C, Clark J E and Koditschek D E 2013 Variable stiffness legs for robust, efficient, and stable dynamic running *J. Mech. Rob.* **5** 011009
- [16] Ananthanarayanan A, Azadi M and Kim S 2012 Towards a bio-inspired leg design for high-speed running *Bioinsp. Biomim.* **7** 046005
- [17] Housner G W et al 1997 Structural control: past, present, and future *J. Eng. Mech.* **123** 897–971
- [18] Jolly M R, Bender J W and Carlson J D 1999 Properties and applications of commercial magnetorheological fluids *J. Intell. Mater. Syst. Struct.* **10** 5–13
- [19] Wang D H and Liao W H 2011 Magnetorheological fluid dampers: a review of parametric modelling *Smart Mater. Struct.* **20** 023001
- [20] Dyke S J, Spencer B F Jr, Sain M K and Carlson J D 1998 An experimental study of MR dampers for seismic protection *Smart Mater. Struct.* **7** 693
- [21] Li W H, Yao G Z, Chen G, Yeo S H and Yap F F 2000 Testing and steady state modeling of a linear MR damper under sinusoidal loading *Smart Mater. Struct.* **9** 95
- [22] Wang D H and Liao W H 2011 Magnetorheological fluid dampers: a review of parametric modelling *Smart Mater. Struct.* **20** 023001

- [23] Jolly M R, Carlson J D and Munoz B C 1996 A model of the behaviour of magnetorheological materials *Smart Mater. Struct.* **5** 607
- [24] Li W H, Wang X Y, Zhang X Z and Zhou Y 2009 Development and analysis of a variable stiffness damper using an MR bladder *Smart Mater. Struct.* **18** 074007
- [25] Phillips R W 1969 Engineering applications of fluids with a variable yield stress *Doctoral Dissertation* (Berkeley: University of California)
- [26] Paciello V and Pietrosanto A 2011 Magnetorheological dampers: a new approach of characterization *IEEE Trans. Instrum. Meas.* **60** 1718–23
- [27] Iagnemma K, Kang S, Shibly H and Dubowsky S 2004 Online terrain parameter estimation for wheeled mobile robots with application to planetary rovers *IEEE Trans. Rob.* **20** 921–7
- [28] Weingarten J D, Groff R E and Koditschek D E 2004 A framework for the coordination of legged robot gaits *RAM: IEEE Conf. on Robotics, Automation and Mechatronics* vol 2pp 679–86
- [29] Seok S, Wang A, Chuah M Y, David Otten D, Lang J and Sangbae Kim S 2013 Design principles for highly efficient quadrupeds and Implementation on the MIT cheetah robot *ICRA: IEEE Conf. on Robotics and Automation* pp 3307–12